Method for Estimation of Refractive Index and Size Distribution of Aerosol Using Direct and Diffuse Solar Irradiance as well as Aureole by Means of a Modified Simulated Annealing

March 2005

Department of Engineering Systems and Technology
Graduate School of Science and Engineering
Saga University

XingMing Liang

Abstract

A multistage method for estimation of the refractive index and the size distribution of aerosol using direct and diffuse solar irradiance as well as aureole by means of a method of the modified simulated annealing is proposed. In this method, based on simulated annealing, a gradually decreasing oscillation function is introduced into the temperature of annealing in order to acceralate learning process of annealing. By using the method of Successive Orders of Scattering, the simulated data of direct and diffuse solar irradiance are generated together. Meanwhile, aureole irradiance is estimated by means of an empirical method from the experimental data. A comparison between the existing method, which is based on linear inversion method proposed by P. Romanov et.al, and the proposed method is made. The results show that the retrieval precisions from the proposed method improved twice more than that in the existing method.

Keywords: Aerosol, Aureole, Refractive Index, Size Distribution, Simulated Annealing, Annealing Temperature, Successive Orders of Scattering.

Contents

Figure Index

Table Index

Chapter 1

Introduction

Romanov et al.(1999), Sherbrooke University proposed a method for estimation of the refractive index and the size distribution of aerosol by means of linear inversion method. They estimated the refractive index and the size distribution of aerosol for the atmospheric column from the measured data of diffuse solar irradiance at surfaces, aureole(solar peripheral irradiance) at surfaces and aerosol optical depth as a solution of linear inversion method(It is referred to ”Sherbrooke Model” hereafter). However, the relation between unknown parameters(the size distribution and the refractive index) and measurement data(diffuse solar irradiance, aureole and optical depth of aerosol) is not linear, thus the estimation accuracy is not sufficient.

A sensitivity analysis is made for the Sherbrooke model with respect to the retrieval accuracy on each variable. Through the analysis, it is shown that the sensitivities of the real part of the refractive index and the size distribution are good enough while that of the imaginary part of the refractive index is not. Thus it is also shown that estimation accuracy of the imaginary part of the refractive index is not good enough in comparison to those for the real part of the refractive index and the size distribution. It is caused by a non-linear relation between the unknown parameters and the measurement data as well as a small influence due to the imaginary part of the refractive index compared to the real part of the refractive index and the size distribution. Thus a method for estimation of the aerosol size distribution and the refractive index based on nonlinear inversion is proposed together with multi-stage estimation of which firstly the unknown parameters which show relatively high sensitivities are estimated followed by the rest of unknown parameters(It is referred to Arai-Ryo model).

With respect to the methods of the nonlinear inversion, there are various iterative methods, such as Jacobi Method, SDM(Steepest Descent Method), CGM(Condjugate Gradient Method) , SA(the method simulated annealing), and so on. they can not avoid getting local minima for most of the methods except simulated annealing which ensure

to reach global optimum solution theoretically (Arai,2001). Meanwhile, it requires anomalous computing resources usually so that an acceleration of learning process is needed. Usually a monotonically decreasing function is used for annealing temperature control in learning process. This may cause a time consuming process. In this thesis, a monotonically decreasing oscillation function is introduced for annealing temperature control. A monotonically decreasing function ensure to reach a global optimum solution while an oscillation function makes to reach a optimum solution much faster and also makes to come out from local minima.

In order to make a sensitivity analysis as well as evaluation of estimation accuracy of both Sherbrooke Model and Arai-Ryo models, the simulated and/or the observed data of direct and diffuse solar irradiance at surfaces as well as aureole are needed. A successive orders of scattering method is used for generation of the simulated direct and diffuse solar irradiance data with the varieties of the aerosol parameters(Guang-Yu Shi,1998) of the refractive index and the size distribution. Meanwhile, aureole is calculated based on an empirical model(Box et al,1981) proposed by P. Romanov of Sherbrooke University. Using the simulation data, it is shown the sensitivities of the real part of the refractive index and the size distribution are good enough while that of the imaginary part of the refractive index is not, and it also shown Arai-Ryo model is superior to the Sherbrooke model in terms of estimation accuracy.

To generate the simulated data of diffuse irradiance, we will describe in detail the solution of the radiative transfer equation by means of the method of successive orders of scattering in chapter 2. We will also discuss the influence on the diffuse irradiance due to the surface and the atmospheric media in this chapter. Atmospheric optical properties will be described in chapter 3. We will discuss the phase functions of atmospheric molecule and aerosol particle based on the theories of Rayleigh scattering and Mie scattering, meanwhile, we will explain how to calculate the optical depth of aerosol particles from their microphysics properties. In addition, we will describe simply the absorption from water vapor and ozone in visible and near-infrared spectral range in this chapter. In chapter 4, we will discuss the aureole model based on an empirical model(Box et al,1981) proposed by P. Romanov of Sherbrooke University.

The three chapters above, describe the foundational theories for this thesis. In the later chapters we will devote ourselves to discuss and analyze proposed method. In chapter 5, we will describe in detail Sherbrooke model in which the size distribution and

the refractive index of aerosol are estimated by means of a linear inverse method. A sensitivity analysis is made for the Sherbrooke model with respect to the retrieval accuracy on each variable in chapter 6. It will be shown that the sensitivities of the real part of the refractive index and the size distribution are good enough while that of the imaginary part of the refractive index is not. Thus it will be also shown that estimation accuracy of the imaginary part of the refractive index is not good enough in comparison to those for the real part of the refractive index and the size distribution. In chapter 7 we will discuss in detail the proposed method which the size distribution and the refractive index of aerosol were estimated by means of a modified simulated annealing method. In this chapter, we firstly will summarize simply the method of simulated annealing, then, it will be explained that some faults exist in simulated annealing method and a modified annealing temperature will be introduced into the proposed method for reducing time consumption, finally we will give a whole algorithm of Arai-Ryo model which proposed in the thesis. A comparison of retrieval error between Sherbrooke model and the proposed method will be made in chapter 8. We will also discuss the influence for the retrieval error due to the surface reflectance. In last chapter, we will conclude some views from previous analysis.

Chapter 2

Solving Radiative Transfer Equation

There are many different methods are available to solve radiative transfer equation, such as DOM(Discrete Ordinates Method), SOS(Successive Orders of Scattering), Gauss-Seidel Iteration, Doubling and Adding Method, and so on. In this thesis, we will mainly introduce one of them for the radiative transfer problem: SOS. It was chosen for two main reasons; 1) it is physically intuitive, especially as the physics remains clear through the mathematical formalism, and hence relatively easy to code; and 2) it is easily adaptable to different geometries and types of simulations.

In the following three sections, we firstly describe simply the concept of the radiative transfer equation. Then, we explain in detail the method of SOS for a plane-parallel atmosphere. Finally, we discuss two factors that affect the radiative transfer equation: the surface reflectance and the atmospheric media.

2.1 Radiative Transfer Equation

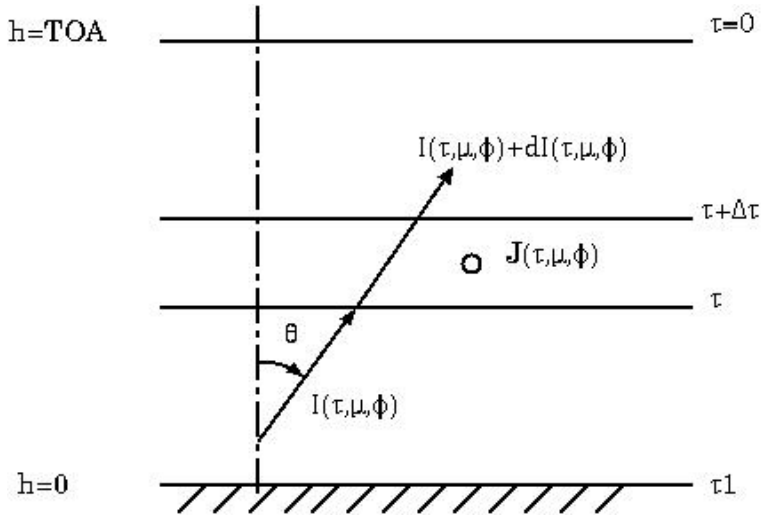

Fig.2. 1 Concept of the Radiative Transfer.

The equation of the radiative transfer for the diffuse irradiance $I(\tau,\mu,\phi)$ in a plane-parallel scattering media that is shown as Fig.2.1 may be written,

$$\mu\frac{dI(\tau,\mu,\phi)}{d\tau} = I(\tau,\mu,\phi) - J(\tau,\mu,\phi) \tag{2.1}$$

The optical depth τ is the measured perpendicular to the media boundaries with τ=0 at TOA(Top of Atmosphere), and the direction is specified through μ (absolute value of the cosine of the zenith angle) and ϕ(the azimuth angle). In this thesis, the source term $J(\tau,\mu,\phi)$ is defined by:

$$J(\tau,\mu,\phi) = \frac{\varpi}{4\pi}\int_{-1}^{1} d\mu' \int_{0}^{2\pi} d\phi' P(\tau,\mu,\phi,\mu',\phi') I(\tau,\mu',\phi') + J_{beam} + J_{thermal} \tag{2.2}$$

The source term J_{beam} corresponds to scattering of a parallel beam of incident flux $\mu_0 F_0$ in direction (μ_0,ϕ_0). $J_{thermal}$ represents the thermal emission (assumed isotropic) which determined by a Planck function $B(T)$ at temperature T, specifically .

$$J_{beam} = \frac{\varpi}{4\pi} P(\mu,\phi,-\mu_0,\phi_0) F_0 e^{-\tau/\mu_0} \tag{2.3}$$

$$J_{thermal} = (1-\varpi)B(T) \tag{2.4}$$

where $P(\mu,\phi,\mu',\phi') = P(\Theta)$ is the phase function for the scattering media, which depends on scattering angle Θ, and ϖ is the single scattering albedo. The scattering angle is given in terms of (incident and scattered) directional variables through the usual relation:

$$\cos(\Theta) = -\mu\mu' + \sqrt{(1-\mu^2)(1-\mu'^2)}\cos(\phi-\phi') \tag{2.5}$$

In visible and near-infrared spectral region the contribution of thermal emission processes to the source function can be negligible, and thus, the source function comprise only scattering processes. Substituting Eq.(2.3) into Eq.(2.2) and omitting the third term of right side in Eq.(2.2), we can obtain the approximate source function in visible and near-infrared spectral region as follows,

$$J(\tau,\mu,\phi) = \frac{\varpi}{4\pi}\int_{-1}^{1} d\mu' \int_{0}^{2\pi} d\phi' P(\mu,\phi,\mu',\phi') I(\tau,\mu',\phi') + \frac{\varpi}{4\pi} P(\mu,\phi,-\mu_0,\phi_0) F_0 e^{-\tau/\mu_0} \tag{2.6}$$

By means of the method SOS, we can resolve the diffuse irradiance $I(\tau,\mu,\phi)$ from the equation of the radiative transfer Eq(2.1). It describe as the following section.

2.2 Method of Successive Orders of Scattering

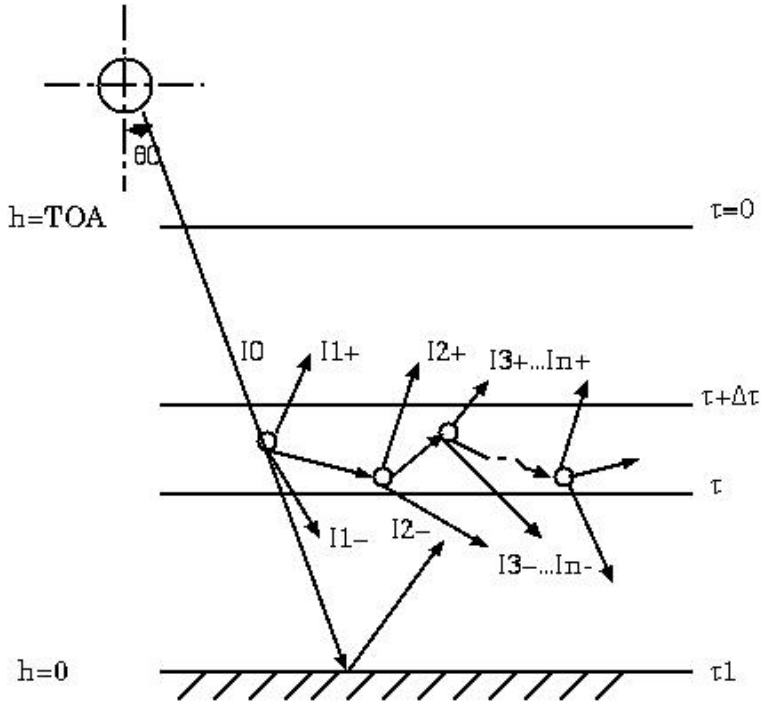

Fig.2. 2 Concept of the Method of Successive Orders of Scattering

The method of SOS is one in which the intensity is computed individually for photons scattered once, twice, three times and so forth, shown as Fig.2.2, with the total intensity obtained as the sum over all orders. Hence for diffuse reflected and transmitted intensities we may write, respectively,

$$I(\tau,\mu,\phi)=\sum_{n=1}^{\infty}I_n(\tau,\mu,\phi) \tag{2.7}$$

$$I(\tau,-\mu,\phi)=\sum_{n=1}^{\infty}I_n(\tau,-\mu,\phi) \tag{2.8}$$

where n denotes the order of scattering.

When we assume that there are no downward diffuse irradiance on the TOA and upward diffuse irradiance on the base of the finite atmosphere, i.e.,

$$I(0,-\mu,\phi) = 0 \tag{2.9}$$

$$I(\tau_1,-\mu,\phi) = 0 \tag{2.10}$$

With the assumed boundary conditions, we have the solution of the equation of radiative transfer as follow,

$$I(\tau,\mu,\phi) = \int_{\tau}^{\tau_1} J(\tau',\mu,\phi)\exp(-(\tau'-\tau)/\mu)\frac{d\tau'}{\mu} \tag{2.11}$$

$$I(\tau,-\mu,\phi) = \int_{0}^{\tau} J(\tau',-\mu,\phi)\exp(-(\tau-\tau')/\mu)\frac{d\tau'}{\mu} \tag{2.12}$$

The zero-order intensity can be given by Dirac's δ function,

$$I_0(\tau,\mu',\phi') = \pi F_0 \exp(-\tau/\mu_0)\delta(\mu'-\mu)\delta(\phi'-\phi) \tag{2.13}$$

Consider the emergent radiation as consisting of light which has been scattered only once. Then, the radiation source is simple,

$$J_1(\tau,\mu,\phi) = \frac{\varpi}{4\pi}\pi F_0 P(\tau,\mu,\phi,\mu_0,\phi_0)\exp(-\tau/\mu_0) \tag{2.14}$$

Inserting it into the formal equations of transfer(Eq. (2.11) and Eq.(2.12)) and integrating over the appropriate optical depths, we obtain intensities due to photons scattered once. It follows that the source and intensities may be derived successively by means of the recursion relationships,

$$I_n(\tau,\mu,\phi) = \int_{\tau}^{\tau_1} J_n(\tau',\mu,\phi)\exp(-(\tau'-\tau)/\mu)\frac{d\tau'}{\mu} \tag{2.15}$$

$$I_n(\tau,-\mu,\phi) = \int_{0}^{\tau} J_n(\tau',-\mu,\phi)\exp(-(\tau-\tau')/\mu)\frac{d\tau'}{\mu} \tag{2.16}$$

$$J_{n+1}(\tau,\mu,\phi)=\frac{\varpi}{4\pi}\int_0^{2\pi}\int_{-1}^{1}P(\tau,\mu,\phi,\mu',\phi')I_n(\tau,\mu',\phi')d\mu'd\phi' \qquad n\geq 1 \qquad (2.17)$$

2.3 Atmospheric Media and Surface Reflection

Atmospheric constituents have a great influence on the radiative transfer by changing the atmospheric optical depth and the phase functions. The atmospheric optical depth from the latitude *h1* to *h2* can be defined as follows,

$$\tau=\int_{h_2}^{h_1}k\rho dh \qquad (2.18)$$

where ρ is the density of the atmospheric constituents. *k* is extinction factor.

In this thesis, we assume that the atmospheric constituents consist of molecule, aerosol, water vapor and ozone, and are homogeneous in parallel direction. Then total optical depth can be written,

$$\tau=\tau_{aer}+\tau_{mol}+\tau_{o3}+\tau_{h2o} \qquad (2.19)$$

$\tau_{mol},\tau_{aer},\tau_{h2o},\tau_{o3}$ represent the optical depths of atmospheric molecule, aerosol, water vapor and ozone, respectively. In general, we can observe immediately the optical depth of water vapor and ozone as well as the total atmosphere. The optical depth of the molecule can also be calculated using an empirical formula described by the chapter 3. So we can obtain the optical depth of aerosol from Eq. (2.19). We also can calculate the optical depths of the different atmospheric constituents using MODTRAN code in different atmospheric models. MODTRAN(Moderate Resolution Transmittance Code) is a code which is capable of predicting atmospheric transmittance and irradiance for frequencies from 0 to 50,000cm^{-1} at moderate spectral resolution, it was developed by AFGL(Air Force Geophysics Laboratory, USA) from 1970. Fig.2.3 shows the optical depths of the four components in visible and infrared spectral range, and they were calculated by MODTRAN4.0. In Fig.2.3 the signs [x] are the measurement data of the total optical depths with resprct to the wavelengths 0.5, 0.675, 0.870 and 1.020um at Saga University in Sep, 2003. we can find that the calculated data of the total optical depths are similar with their values.

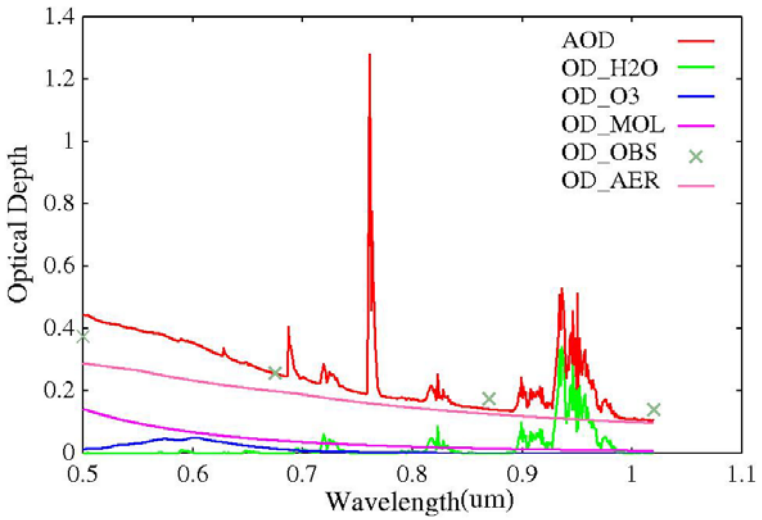

Fig.2. 3 Wavelength Dependence on the Optical Depths.The optical depths of aerosol, molecule, water vapor and O3as well as total of them in visible and infrared spectral range.

We can separate the atmosphere to discrete layers in perpendicular direction as it is heterogeneous. The optical depth of each layer can be written,

$$\tau_i = \tau_{aer,i} + \tau_{mol,i} + \tau_{o3,i} + \tau_{h2o,i} \tag{2.20}$$

where i is the number of atmospheric layer.

If we know the profiles of each atmospheric constituent and the optical depths can be obtained by the ground-based measurement and some empirical formula, the optical depths of each layer can be calculated as follows,

$$\tau_{i,mat} = \frac{\int_{h_{i-1}}^{h_i} \rho(i,mat)dh}{\int_0^{\infty} \rho(i,mat)dh} \tau_{mat} \tag{2.21}$$

Where *mat* represents atmospheric molecule, aerosol, water vapor or ozone, and h is altitude. $\rho(i,mat)$ is the density of component *mat* in the i^{th} atmosphere layer.

Table 2.1 shows the profiles of molecule, aerosol, water vapor and ozone, in which the atmosphere is separated to 30 discrete layers from surface to 50km (McClatchey et. al,1972). It was in Middle-Summer model and aerosol type is assumed as clear model. Fig.2.4 shows the altitude dependence on the optical depths from MODTRAN4.0.

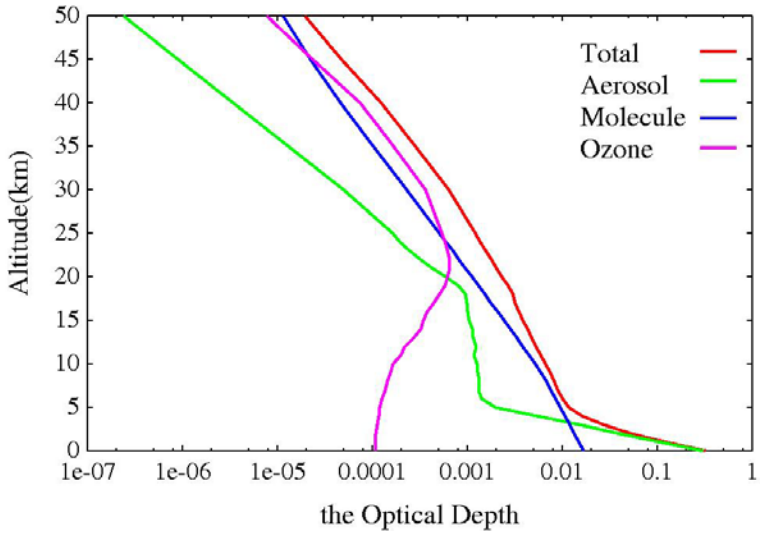

Fig.2. 4 The Altitude Dependence on the Optical Depth.

In Fig.2.4 we can found that aerosol optical depth is contributed mainly by the aerosol particles in the troposphere which the latitude is less than 5*km*, but ozone optical depth is contributed mainly in the stratosphere.

In generation, we can omit the optical depths of the ozone and the water vapor in visible and infrared spectral range as we resolve the radiative transfer equation.

Although we assume the upwelling diffuse irradiance as 0 at surface in Eq.(2.10), actually, it is great influenced by the surface reflection. Here, we assume the surface as Lanbertian surface, so the upwelling diffuse irradiances at surface in all of the scattering angles are the same and can be written with a surface reflectance(A) as follows.

$$I(\tau_1,\mu,\phi)=\frac{A}{\pi}\int_0^{2\pi}\int_0^1 I(\tau_1,-\mu',\phi')\mu' d\mu' d\phi' \tag{2.22}$$

Table 2. 1 Atmospheric Profiles in Urban Type.

Atompheric Profile						Clear model
Antitude	Press	Temp	Molecule	Water vapor	Ozone	Aerosol
km	atm	K	gm/m3	gm/m3	gm/m3	cm-3
0	1012.882	294.2	1.301E+03	1.40E+01	6.00E-05	1.378E+04
1	901.912	289.7	1.162E+03	9.293E+00	6.00E-05	5.030E+03
2	801.936	285.2	1.037E+03	5.896E+00	6.00E-05	1.844E+03
3	709.957	279.2	9.230E+02	3.296E+00	6.20E-05	6.731E+02
4	627.974	273.2	8.282E+02	1.899E+00	6.40E-05	2.453E+02
5	553.988	267.2	7.411E+02	9.995E-01	6.60E-05	8.987E+01
6	487.000	261.2	6.614E+02	6.100E-01	6.90E-05	6.337E+01
7	426.000	254.7	5.886E+02	3.696E-01	7.50E-05	5.890E+01
8	372.000	248.2	5.222E+02	2.099E-01	7.90E-05	6.069E+01
9	324.000	241.7	4.619E+02	1.199E-01	8.60E-05	5.818E+01
10	281.000	235.3	4.072E+02	6.396E-02	9.00E-05	5.675E+01
11	243.000	228.8	3.496E+02	2.199E-02	1.10E-04	5.317E+01
12	209.000	222.3	2.999E+02	5.997E-03	1.20E-04	5.585E+01
13	179.000	215.8	2.572E+02	1.438E-03	1.50E-04	5.156E+01
14	153.000	215.7	2.206E+02	7.684E-04	1.80E-04	5.048E+01
15	130.000	215.7	1.890E+02	4.440E-04	1.90E-04	4.744E+01
16	111.000	215.7	1.620E+02	3.680E-04	2.10E-04	4.511E+01
17	95.000	215.7	1.388E+02	3.054E-04	2.40E-04	4.458E+01
18	81.200	216.8	1.188E+02	2.556E-04	2.80E-04	4.314E+01
19	69.500	217.9	1.017E+02	2.211E-04	3.20E-04	3.634E+01
20	59.500	219.2	8.690E+01	1.941E-04	3.40E-04	2.667E+01
21	51.000	220.4	7.421E+01	1.730E-04	3.60E-04	1.933E+01
22	43.700	221.6	6.338E+01	1.538E-04	3.60E-04	1.455E+01
23	37.600	222.8	5.415E+01	1.408E-04	3.40E-04	1.113E+01
24	32.200	223.9	4.624E+01	1.246E-04	3.20E-04	8.826E+00
25	27.700	225.1	3.950E+01	1.120E-04	3.00E-04	7.429E+00
30	13.200	233.7	1.783E+01	5.752E-05	2.00E-04	2.238E+00
35	6.520	245.2	7.924E+00	2.852E-05	9.20E-05	5.890E-01
40	3.330	257.5	3.625E+00	1.429E-05	4.10E-05	1.550E-01
45	1.760	269.9	1.741E+00	7.700E-06	1.30E-05	4.082E-02
50	0.951	275.7	8.954E-01	4.111E-06	4.30E-06	1.078E-02

Chapter 3

Atmospheric Optical Properties

The optical properties(e.g, optical depth, single scattering albedo, phase function) of the medium are determined by the particles that compose the medium and their properties. If the molecular particles in the atmosphere are far smaller than the wavelength, its scattering pattern can be calculated by the Rayleigh scattering law. For spherical particles, their scattering behaviors depend on the refractive index and size parameter defined as follows,

$$\chi = \frac{2\pi r}{\lambda} \tag{3.1}$$

Where r is the radius of sphere. In the following two sections, we discuss scattering theory for both small particles(Rayleigh scattering) and large particles(Mie scattering) in order to calculated the optical depth and phase function of atmospheric media.

3.1 Rayleigh Scattering

If χ is smaller than 0.01, then the Rayleigh scattering formulas are valid. The phase function for Rayleigh particles can be written as follows,

$$P(\Theta) = \frac{3}{8\pi(2+\Delta)}((1+\Delta)+(1-\Delta)\cos^2(\Theta)) \tag{3.2}$$

where $\triangle$ is the depolarization factor that gives the correction for the depolarization effect of scattering from anisotropic molecules.

The optical depth of Rayleigh scattering can be calculated by MODTRAN described above. It also can be calculated by using an empirical formula proposed by the 2th

WMO Conference. It is shown as follows,

$$\tau_{mol} = \frac{P}{1013.26} * 0.00838\lambda^{-(3.916+0.074\lambda+\frac{0.005}{\lambda})} \tag{3.3}$$

where P is atmosphere press and λ is wavelength in unit *um*.

3.2 Aerosol Scattering

If the particle size is very close to the length of the wavelength (i.e., $0.1<\chi<50$), such as the most aerosol particles in the atmosphere, their scattering behavior can be characterized by Mie theory. Here we only introduce phase function and optical depth of the particle by Mie scattering.

The exact expression for the element of the amplitude scattering matrix for isotropic spherical particles illuminated by a linearly polarized plane electromagnetic wave are ,

$$s_{11}(\Theta) = \sum_{n=1}^{\infty} \frac{2n+1}{n(n+1)} (a_n \tau_n(\cos(\Theta)) + b_n \pi_n(\cos(\Theta))) \tag{3.4}$$

$$s_{22}(\Theta) = \sum_{n=1}^{\infty} \frac{2n+1}{n(n+1)} (a_n \pi_n(\cos(\Theta)) + b_n \tau_n(\cos(\Theta))) \tag{3.5}$$

$$s_{12}(\Theta) = s_{21}(\Theta) = 0 \tag{3.6}$$

where

$$a_n = \frac{\psi_n{}'(m\chi)\psi_n(\chi) - m\psi_n(m\chi)\psi_n{}'(\chi)}{\psi_n{}'(m\chi)\xi_n(\chi) - m\psi_n(m\chi)\xi_n{}'(\chi)} \tag{3.7}$$

$$b_n = \frac{m\psi_n{}'(m\chi)\psi_n(\chi) - \psi_n(m\chi)\psi_n{}'(\chi)}{m\psi_n{}'(m\chi)\xi_n(\chi) - \psi_n(m\chi)\xi_n{}'(\chi)} \tag{3.8}$$

where $m = \kappa - \eta i$ is the refractive index of the spherical particle. The real part(κ) is commonly called refractive index and the imaginary part(η) repress the absorption of

aerosol particles.

$$\psi_n(\chi) = \sqrt{\pi\chi/2} B_{n+1/2}(\chi) \tag{3.9}$$

$$\xi_n(\chi) = \sqrt{\pi\chi/2} H_{n+1/2}(\chi) \tag{3.10}$$

where $B_{n+1/2}(\chi)$ and $H_{n+1/2}(\chi)$ are the Bessel and Hankel functions. The angle functions are determined by the following formulas,

$$\pi_n(\cos(\Theta)) = \frac{P_n^1(\cos(\Theta))}{\sin(\Theta)} \tag{3.11}$$

$$\tau_n(\cos(\Theta)) = \frac{dP_n^1(\cos(\Theta))}{d\Theta} \tag{3.12}$$

where $P_n^1(\cos(\Theta))$ is the associated Legendre polynomial and Θ is the scattering angle. Then we can calculate some optical properties of particle according to Mie theory as follows,

Extinction efficiency factor:

$$Q_{ext} = \frac{2}{\chi^2} \sum_{n=1}^{\infty} (2n+1) \operatorname{Re}(a_n + b_n) \tag{3.13}$$

Scattering efficiency factor:

$$Q_{sca} = \frac{2}{\chi^2} \sum_{n=1}^{\infty} (2n+1)(|a_n|^2 + |b_n|^2) \tag{3.14}$$

Phase function:

$$P(\Theta) = \frac{2(|s_{11}|^2 + |s_{22}|^2)}{k^2 r^2 Q_{sca}} \tag{3.15}$$

For particles with a size distribution f®, we can calculate the extinction and scattering

coefficients σ_{ext} , σ_{sca} ,phase function $P(\Theta)$, single scattering albedo ω and the scattering optical depth of aerosol τ_{sca} ,

$$\sigma_{ext} = N\int_0^\infty \pi r^2 Q_{ext} f(r)dr \tag{3.16}$$

$$\sigma_{sca} = N\int_0^\infty \pi r^2 Q_{sca} f(r)dr \tag{3.17}$$

$$P(\Theta) = \frac{2\pi N\int_0^\infty (|s_{11}|^2 + |s_{22}|^2) f(r)dr}{k^2 \sigma_{sca}} \tag{3.18}$$

$$\omega = \frac{\sigma_{sca}}{\sigma_{ext}} \tag{3.19}$$

$$\tau_{sca} = \int_z^\infty \sigma_{sca}(z)\rho(z)dz \tag{3.20}$$

If the density of vertical atmospheric constituents are normalized 1, that is,

$$\int_z^\infty \rho(z)dz = 1 \tag{3.21}$$

then the optical depth is equate to the average scattering coefficients $\overline{\sigma_{sca}}$ according to Eq(3.20).

For a group of particles, we need to specify the particle size distribution function ($f(r)$). In general, aerosol particle sizes are not identical. Their radiuses can be represented by many different functions, such as the power-law function, the modified gamma distribution function, and the lognormal distribution function. In this thesis, we selected the power-law (Junge) function as the particle size distribution function, in which the computation of the particle size distribution is simplest. Letting $n(r)dr$ be the number of particles per unit volume in size range r to $r + \Delta r$, this distribution can be expressed as follow,

$$n(r)=\begin{cases} Cr^{-a} & 0.01\mu m < r < 10\mu m \\ 0 & otherwise \end{cases} \tag{3.22}$$

where a is a parameter between 2.5 to 4.0 for the natural aerosols and it is refered to Junge parameter in this thesis.

Fig.3.1 and Fig3.2 show the calculations of some scattering coefficients σ_{sca} and phase functions $P(\Theta)$. In Fig.3.1 we can find that scattering coefficient of the particles without the absorption (the imaginary part is 0) is stable to 2 as the particle radius becomes large. In Fig.3.2 we can find that the phase function of the large particles is extremely asymmetrical and is greatly larger in the forward scattering angles than that in the backward scattering angles. The smallest value of the phase function is about in the scattering angle 120°.

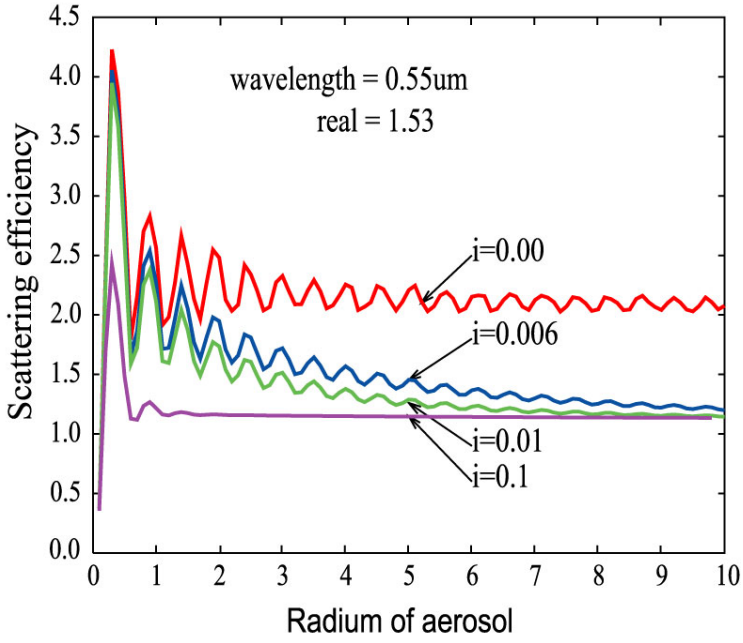

Fig.3. 1 Aerosol Radius Dependence on Scattering Efficiency.

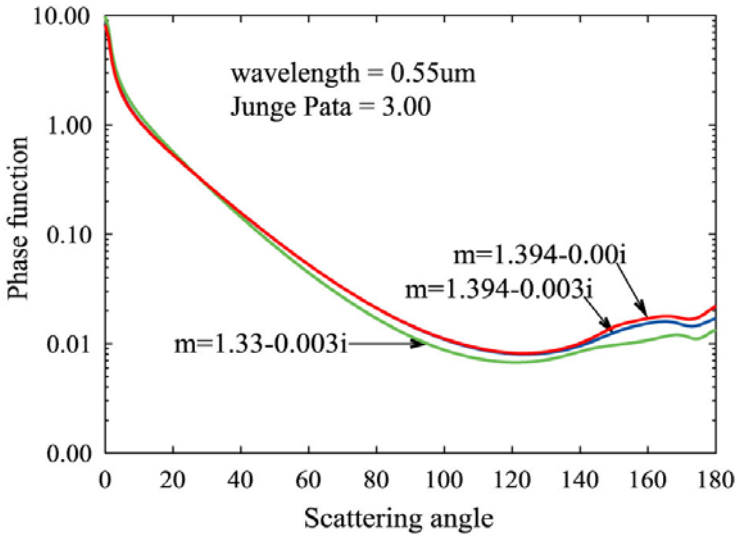

Fig.3. 2 Phase Function of the Aerosol for the Several Refractive Indices (a=3.0).

3.3 Gaseous Absorption

Although the absorption can be omitted in solving the radiative transfer equation in visible and near-infrared spectral region, it is necessary to know the absorption of atmospheric media. The absorption is caused mainly by atmospheric gases, such as water vapor, ozone, oxygen and aerosols. The aerosol absorption is accounted for by the single scattering albedo ω. If ω=1, the aerosols are not absorptive. For most multispectral sensors, we are concerned mainly with water vapor and ozone. From Table 2.1 and Fig.2.4 we can find that ozone is distributed mainly in the stratosphere (20~50km above the surface) but water vapor is in the boundary layer(the lowest is 1~4km). Fig.3.3 show the impacts of water vapor content calculated from Modtran4.0. From this figure, we can see that the impacts are mainly in the longer wavelength. Fig.3.4 shows the impacts of ozone absorption. Fig.3.5. displays the impacts of CO2 and other gases. It is clear that their impacts are mainly in the longer wavelength. The total atmospheric transmittance with the default values of the midlatitude summer in Modtran4.0 is shown in Fig.3.6. This also explains why the contribution of thermal emission processes to the source function almost can be omitted in solving the radiative transfer equation in visible and near-infrared spectral region.

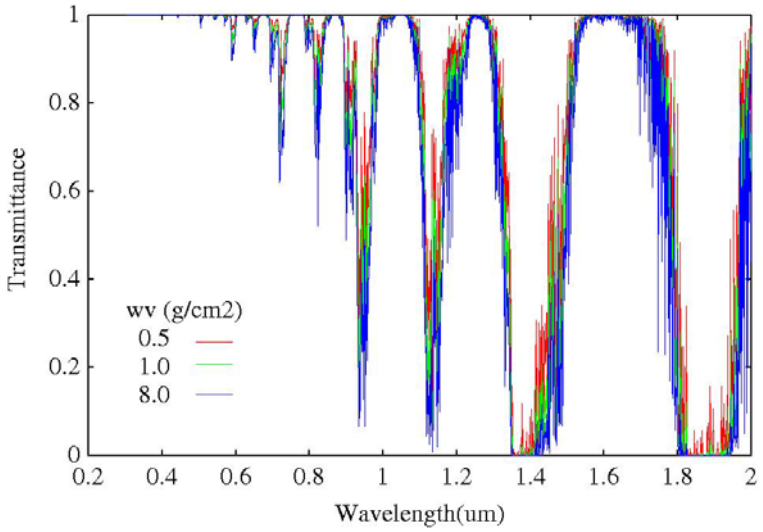

Fig.3. 3 Transmittance of Atmosphere with Different Water Vapor Content.

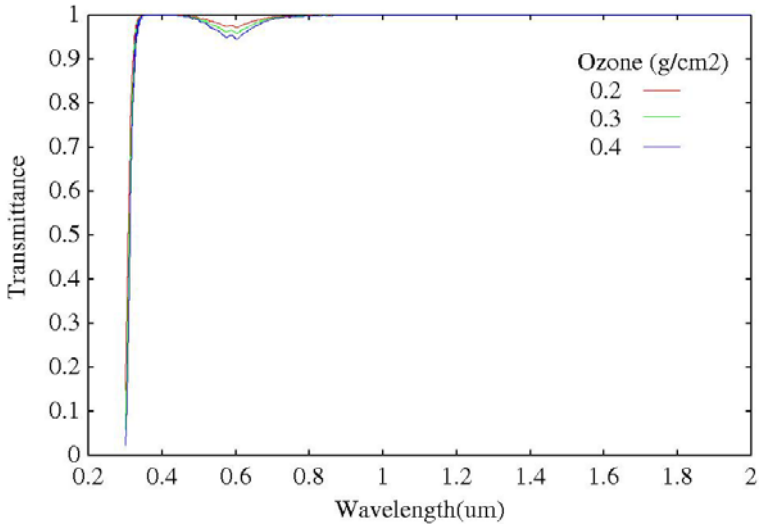

Fig.3. 4 Atmospheric Transmittance with Different Ozone Concentrations.

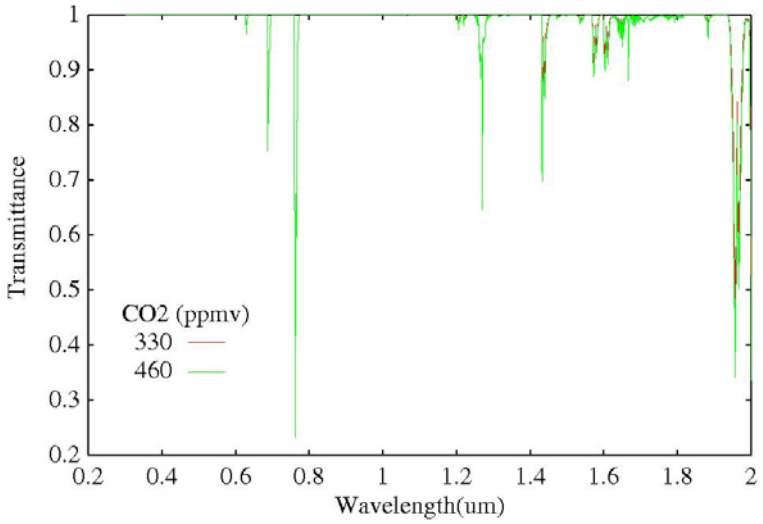

Fig.3. 5 Atmospheric Transmittance with CO2 Concentrations .

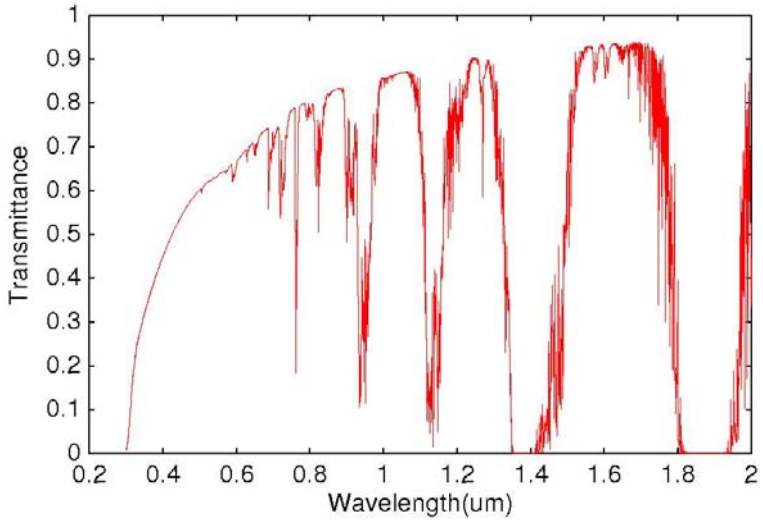

Fig.3. 6 Total Transmittance of a Standard Atmosphere in Modtran4.0.

Chapter 4

Aureole Model

The solar aureole is a region of enhanced brightness within about 20° of the sun's disk, due to the predominant forward-scattering effect of atmospheric aerosols. The solar aureole theory and its use for determining aerosol size distributions also has been discussed in detail by Deirmendjian(1959). Here, we calculated aureole irradiance using MS(multiply scattering) approximation proposed by M.A.Box et.al(1981). They assumed that the solar aureole irradiance was essentially due to SS(single scattering) by aerosols and molecules, and MS by molecules alone. Moreover, they also taken into account the effect of the surface reflectance in the computation of the aureole irradiance. P.Romanov et al.(1999) summarized an empirical formula of aureole irradiance based on the method proposed by M.A.Box et.al. It is shown as follows,

$$I_{aur}(\Theta,\lambda)=\frac{F_0(\lambda)}{\mu_0}\exp(-\frac{\tau(\lambda)}{\mu_0})(\tau_{mol}(\lambda)P_{mol}(\Theta,\lambda)+\tau_{sca}(\lambda)P_{aer}(\Theta,\lambda)+\Delta_{ms}(\Theta,\lambda,A)) \tag{4.1}$$

where $I_{aur}(\Theta,\lambda)$ is the aureole irradiance measured at scattering angle Θ, $P_{mol}(\Theta,\lambda)$ and $P_{aer}(\Theta,\lambda)$ are the Rayleigh and aerosol phase functions, respectively. $\tau_{sca}(\lambda)$ is the aerosol scattering optical depth. $\Delta_{ms}(\Theta,\lambda,A)$ is a term that represents the contribution of the effects of multiple scattering and reflection from the surface in solar aureole. It can be written as follows,

$$\Delta_{ms}(\Theta,\lambda,A)=\tau_A(\lambda,A)P_{mol}(0^0,\lambda)+P_{mol}(\Theta,\lambda)t_{ms} \tag{4.2}$$

Where,

$$\tau_A(\lambda,A)=A\tau_2/(1-A\tau_3),$$

$$\tau_2=1.34\tau_{ss}\mu_0/(1.0+0.22(\tau_{ss}/\mu_0)^2),$$

$$\tau_3=0.9\tau_{ss}-0.92\tau_{ss}^2+0.54\tau_{ss}^3,$$

$$t_{ms} = 0.02\tau_{ss} + 1.2\tau_{ss}^2 / \mu_0^{0.25},$$

$$\tau_{ss} = \tau_R(\lambda) + \tau_{sa}(\lambda) \tag{4.3}$$

A is the surface reflectance and τ_{ss} is the total scattering optical depth.

Fig.4.1 shows a comparison of the calculated result between aureole irradiance from MS model and diffuse irradiance from the method of successive orders of scattering. The aureole irradiance was calculated by the aureole model described as above in an angle range of the forward scattering in which the azimuth angles are from 0° to 30° and the zenith angle is the same as the solar zenith angle. Meanwhile, the diffuse irradiance was calculated in all azimuth angles from 0° to 180° by the method of the successive orders of scattering. In the forward scattering, we found that it was quite different of calculated results between the diffuse irradiance and the aureole irradiance. This is because that it exist not only scattering but also diffraction when light passes particle in the forward direction. It results in generating a region of enhanced brightness in forward direction. From now on, we removed the unrealistic part of diffuse irradiance, and remained the corresponding exact estimates of the aureole irradiance in the forward scattering.

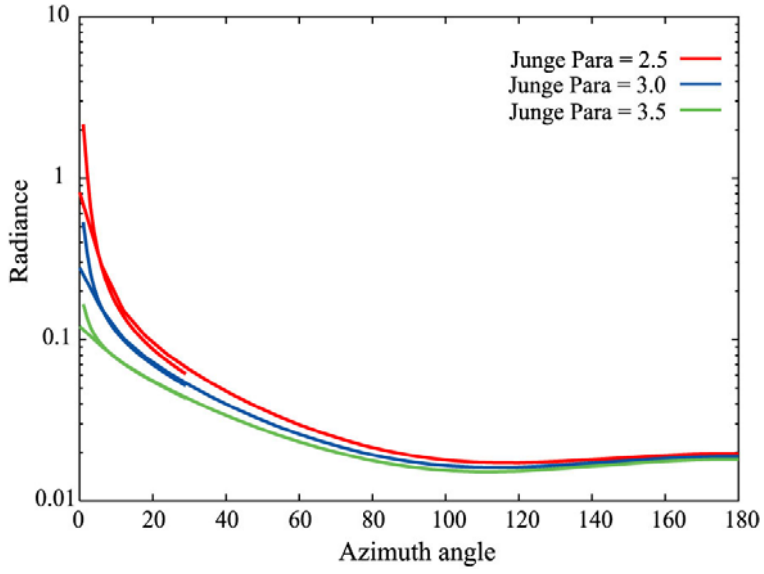

Fig.4. 1 Comparison the Aureole Irradiance from MS Model and Diffuse Irradiance from the Method of Successive Orders of Scattering.

Chapter 5

Sherbrooke Model

The estimation method for the refractive index and the size distribution of aerosol proposed by P.Romanovs of the Sherbrooke University based on linear inversion method is summarized as follows. The aerosol refractive index and size distribution are retrieved by minimizing the squared difference between the measured data and the simulated data of direct solar irradiance at surface (or aerosol optical depth), downward diffuse irradiance at surface and solar peripheral irradiance (aureole) based on the plane-parallel atmospheric model. This model also considered molecular Rayleigh scattering and Mie scattering which is dependence on the aerosol refractive index and size distribution.

First,

$$F = H\varphi + e \tag{5.1}$$

is defined where F is the vector of the deviations of the measured data, that is,

$$F = \begin{pmatrix} I_{dir} - I^{*}_{dir} \\ I_{dif} - I^{*}_{dif} \\ I_{aur} - I^{*}_{aur} \end{pmatrix} \tag{5.2}$$

[*] denotes the measurement data. H is a Jacobian, and can be expressed as,

$$H = \begin{pmatrix} I'_{dir}(\nu 1) & \ldots & I'_{dir}(\nu m) & I'_{dir}(\kappa) & I'_{dir}(\eta) \\ I'_{dif}(\nu 1) & \ldots & I'_{dif}(\nu m) & I'_{dif}(\kappa) & I'_{dif}(\eta) \\ I'_{aur}(\nu 1) & \ldots & I'_{aur}(\nu m) & I'_{aur}(\kappa) & I'_{aur}(\eta) \end{pmatrix} \tag{5.3}$$

where I_{dir} is Solar direct irradiance, I_{dif} is Solar diffuse irradiance and I_{aur} is

aureole irradiance. $I'_{dir}, I'_{dif}, I'_{aur}$ individually indicate a factor of the matrix when the relation between the direct and diffuse solar irradiance and aureole, and the refractive index and size distribution of aerosol is represented as a matrix.

It is also expressed that $E = E_0 \exp(-\tau / \mu_0)$, where E_0 is the exoatmospheric solar irradiance. According to Eq. (2.19), we can replace the direct solar irradiance with aerosol optical depth. From now on, discussion will be focused on aerosol optical depth instead of the direct solar irradiance.

In the formulation of the inverse problem the verctor φ is defined as follows,

$$\varphi^T = \{\varphi_{v1} \cdots \varphi_{vm}, \varphi_\kappa, \varphi_\eta\}$$

$$\varphi_{vm} = s - s^*$$

$$s \in v1, \ldots, vm, \kappa, \eta \tag{5.4}$$

where $v1, \ldots, vm$ represent size distribution of aerosol per air column. κ, η are the real part and the imaginary part of the refractive index.

Because the aerosol optical depth, diffuse solar irradiance and aureole can be measured on the ground, the Eq.(5.2) can be given. It is possible to estimate the unknown parameters of the refractive index and the size distribution of aerosol in the Eq.(5.3). However, because the number of the unknown parameters that represent the size distribution and the real part and the imaginary part of the refractive index is far more than the number of the measured data, it is an ill-posed problem. Hence, it can be solved with commonly used inversion solution based on minimizing norm of estimation error then,

$$\varphi = H^T [HH^T]^{-1} F \tag{5.5}$$

It is well known that the retrieval accuracy of the minimized norm method is not good enough because the number of the unknown parameters is more than it of the equations given. Since the influence of the imaginary part of the refractive index on aureole is so small that the accuracy improvement of the imaginary part of refractive

index can not be expected from this method.

Assuming the aerosol size distribution as Junge distribution, according to Eq.(3.22), the size distribution can be represented as only one Junge parameter(a). Therefore, the Eq.(5.3) can be rewritten as,

$$H = \begin{pmatrix} \tau'_{aer}(a) & \tau'_{aer}(\kappa) & \tau'_{aer}(\eta) \\ I'_{dif}(a) & I'_{dif}(\kappa) & I'_{dif}(\eta) \\ I'_{aur}(a) & I'_{aur}(\kappa) & I'_{aur}(\eta) \end{pmatrix} \tag{5.6}$$

The number of the unknown parameters is three which is totally identical to the number of the equations to be given, so that

$$\begin{pmatrix} \kappa - \kappa^* \\ \eta - \eta^* \\ a - a^* \end{pmatrix} = \begin{pmatrix} \tau'_{aer}(a) & \tau'_{aer}(\kappa) & \tau'_{aer}(\eta) \\ I'_{dif}(a) & I'_{dif}(\kappa) & I'_{dif}(\eta) \\ I'_{aur}(a) & I'_{aur}(\kappa) & I'_{aur}(\eta) \end{pmatrix}^{-1} \begin{pmatrix} \tau_{aer} - \tau^*_{aer} \\ I_{dif} - I^*_{dif} \\ I_{aur} - I^*_{aur} \end{pmatrix} \tag{5.7}$$

The refractive index and Junge parameter can be retrieved simultaneously.

Chapter 6

Sensitivity Analysis

To evaluate the retrieval accuracy of Sherbrooke model, we generate simulated data with the parameters of the refractive index and the size distribution. This simulated data is calculated based on the method of successive orders of scattering, aureole model and Mie theory described as above.

6.1 Atmospheric Assumption and Simulated Data

For generation of the simulated data of diffuse solar irradiance, aerosol optical depth and aureole, it is necessary to assume some atmospheric conditions as follows.

Firstly, the particle was assumed as homogenous ball and the size distribution was a Junge distribution described as chapter 3. It also means that there are not particles in the atmosphere when particle radius is not in the range 0.01*um*~10*um*. Secondly, we supposed atmosphere is homogeneous in horizontal direction but it is inhomogeneous in vertical direction, and the scale of vertical profiles were shown by Table 2.1. Wavelength was selected at 0.55*um*. The Rayleigh scattering optical depth were 0.0943 by assuming a middle latitude summer model in Modtran4.0 with respect to 0.55 μm wavelength. The absorption of the O3 and the water vapor were omitted. After that, we assumed surface as Lanbertian surface and set the surface reflectance is 0.0. the solar zenith angle was assumed as 30° and the azimuth angle was 0° . In addition, we assumed that aureole irradiance was calculated at the solar zenith angle 20° and the azimuth angle 0° . Meanwhile, the direction of the diffuse irradiance was assumed at zenith angle 10° and azimuth angle 180° . The relation of their angles is shown as Fig6.1. In order to generate simulated data of diffuse solar irradiance, aerosol optical depth and aureole, a typical plane-parallel based atmospheric model with the method of successive orders of scattering is used. For improving the retrieval accuracy, the optical depth increment of the adjacent layers is set as less than 0.0005. The layers of atmosphere are set in Table 6.1.

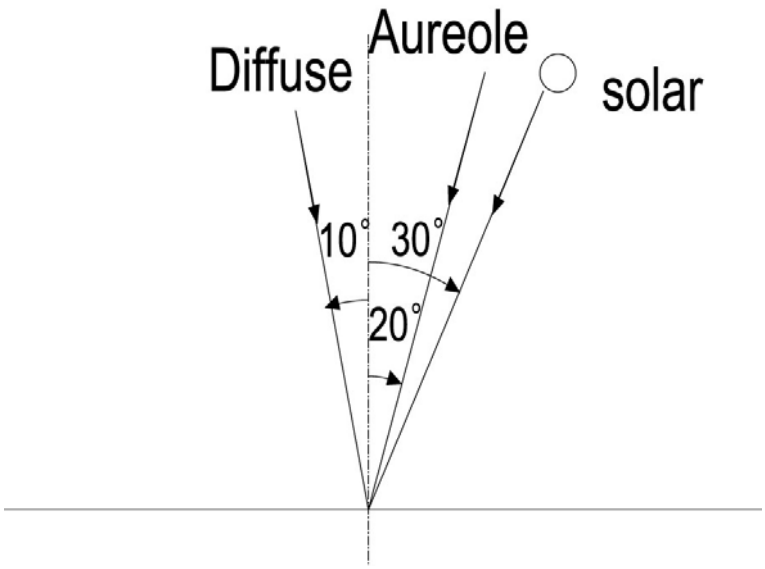

Fig.6. 1 The Direction of Solar, Diffuse Irradiance and Aureole.

.

Table 6. 1 Layered Structure of the Plane Parallel Atmosphere.

Alatitude(km)	Number of Layers	Layer Hight(km)	$\triangle\tau$
0–1	500	0.002	0.00048
1–2	200	0.005	0.00053
2–3	100	0.01	0.00046
3–6	100	0.03	0.00037
6–11	100	0.05	0.00025
11–17	100	0.06	0.00026
17–20	40	0.075	0.00026
20–23	20	0.15	0.00025
23–25	10	0.2	0.00017
25–30	10	0.5	0.00017
30–35	5	1	0.00019
35–50	5	5	0.0001

6.2 Sensitivity Analysis

The real part and the imaginary part of aerosol refactive index and Junge parameters are set in the following ranges,

- The range of the real part of the refractive index is 1.2~1.55.
- The range of the imaginary part of the refractive index is 0.0~0.009,
- The range of the Junge parameter is 2.8~3.15.

Fig.6.2 shows the dependence of the measurement data on the each parameter, (a), (b) and (c) show the dependence of the optical depth of aerosol on the real part, the imaginary part and Junge parameter. (d), (e) and (f) show the dependence of the diffuse irradiance on the parameters. (g), (h) and (i) show the dependence of aureole irradiance on the parameters. It is obvious that the exoatmospheric solar irradiance is assumed to be 1 in the calculation so that the real values can be estimated if the actual exoatmospheric irradiance is considered.

To analyze the sensitivities for the size distribution and the refractive index, we define the sensitivity as follows,

$$S = |(R - R_0)/(x/x_0 - 1)| \tag{6.1}$$

where R , R_0 represent the measurement data of direct, diffuse solar irradiance and aureole and, x , x_0 are the parameters of the real part and the imaginary part of the refractive index as well as Junge parameter. Assuming that the relation between the measurement data and the parameters are linear as the parameters are near to the x_0 , we calculated the sensitivities of the measurement data on the parameters by Eq. (6.1). The results from the sensitivities of the measurement data are shown in Table 6.2.

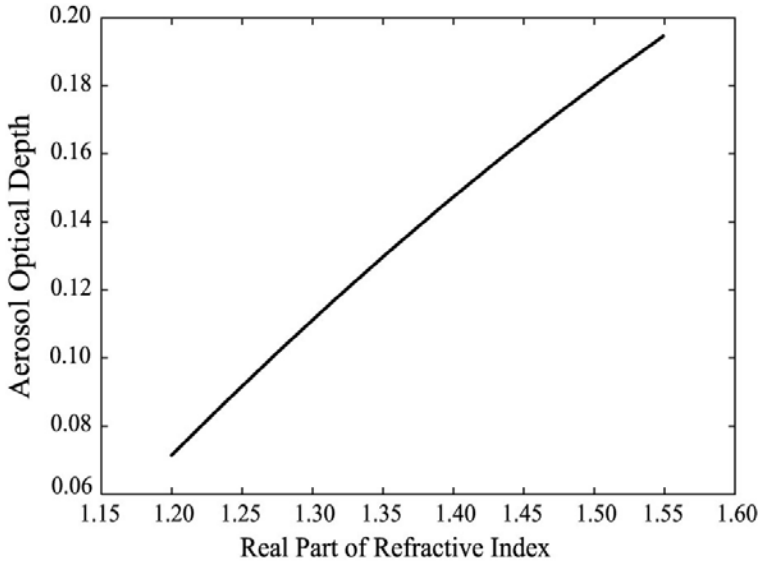
Aerosol Optical Depth
0.20
0.18
0.16
0.14
0.12
0.10
0.08
0.06
1.15
1.20
1.25
1.30
1.35
1.40
1.45
1.50
1.55
1.60
Real Part of Refractive Index

(a)

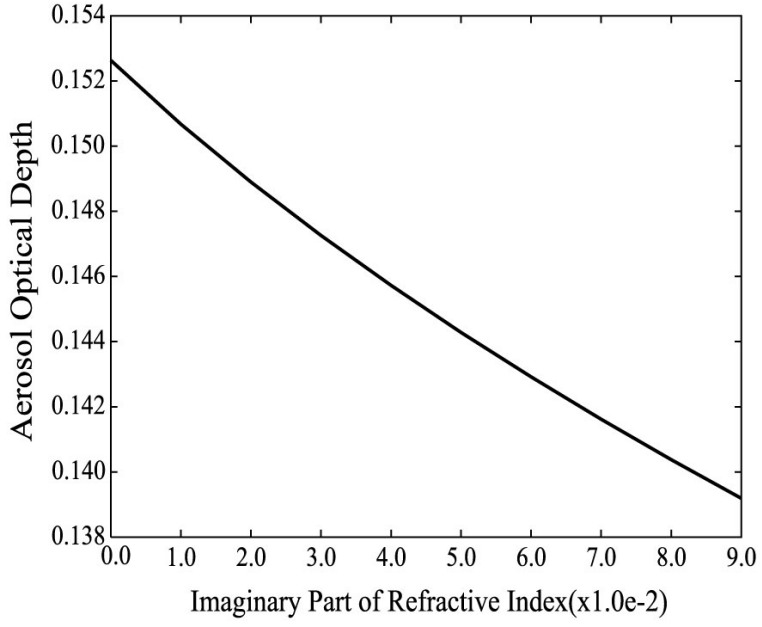
Aerosol Optical Depth
0.154
0.152
0.150
0.148
0.146
0.144
0.142
0.140
0.138
0.0
1.0
2.0
3.0
4.0
5.0
6.0
7.0
8.0
9.0
Imaginary Part of Refractive Index(x1.0e-2)

(b)

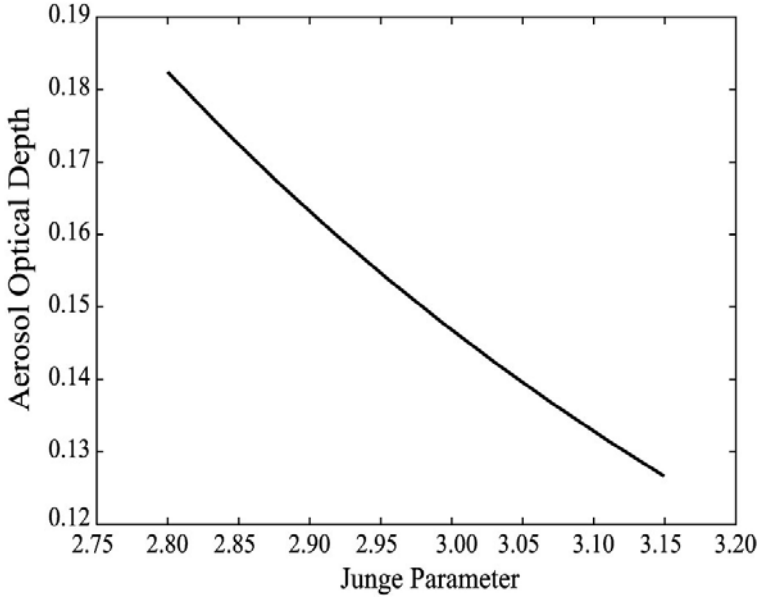
Aerosol Optical Depth
0.19
0.18
0.17
0.16
0.15
0.14
0.13
0.12
2.75 2.80 2.85 2.90 2.95 3.00 3.05 3.10 3.15 3.20
Junge Parameter

(c)

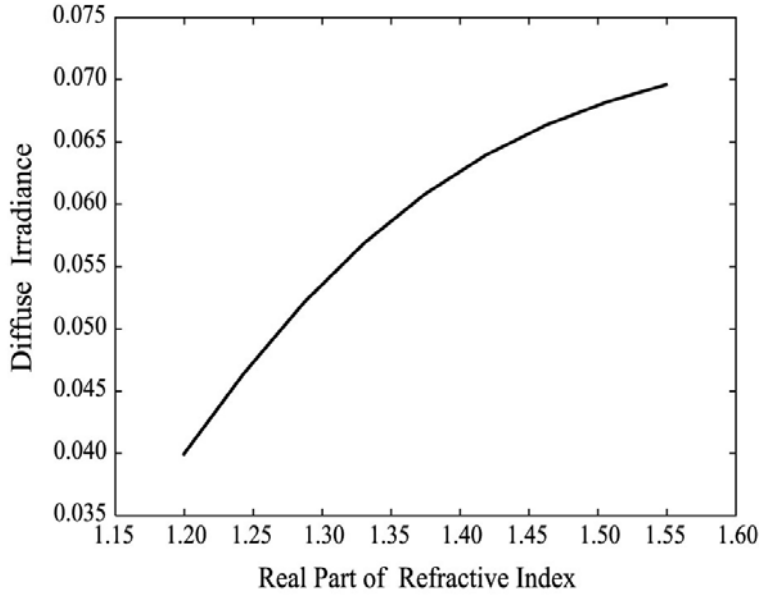
Diffuse Irradiance
0.075
0.070
0.065
0.060
0.055
0.050
0.045
0.040
0.035
1.15 1.20 1.25 1.30 1.35 1.40 1.45 1.50 1.55 1.60
Real Part of Refractive Index

(d)

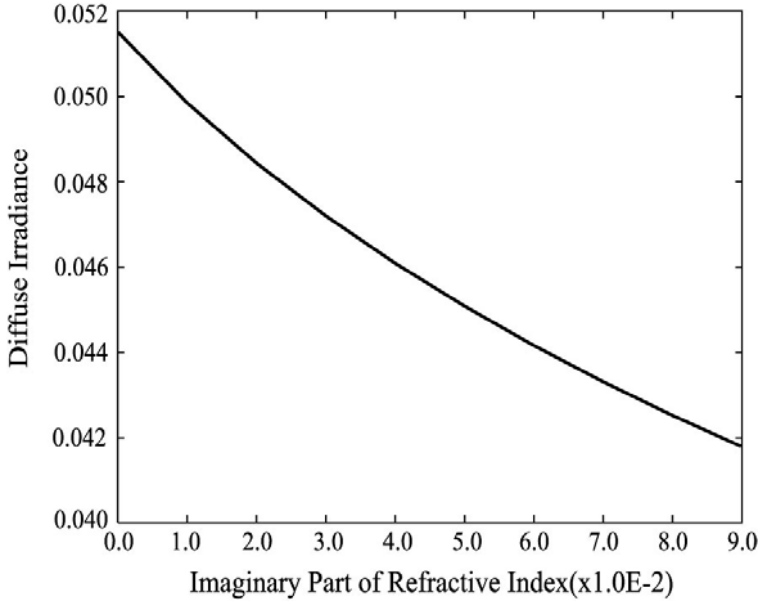
0.052
0.050
0.048
0.046
0.044
0.042
0.040
Diffuse Irradiance
0.0
1.0
2.0
3.0
4.0
5.0
6.0
7.0
8.0
9.0
Imaginary Part of Refractive Index(x1.0E-2)

(e)

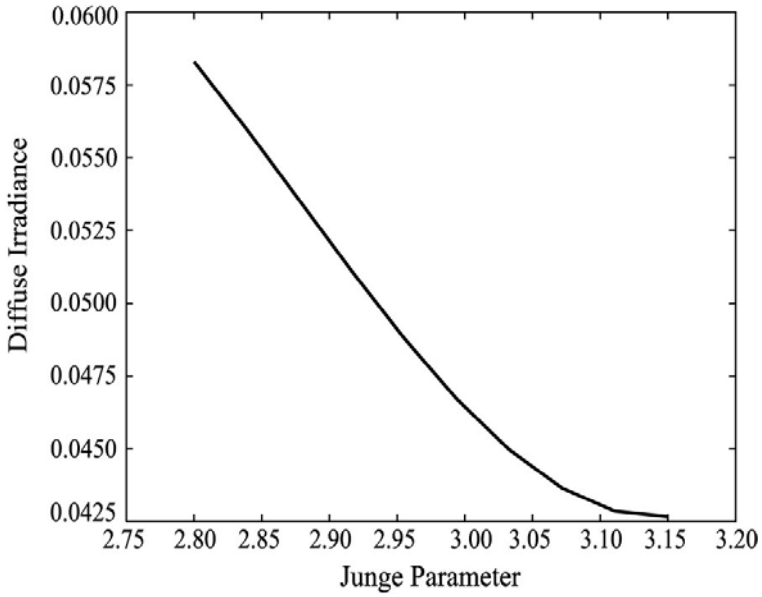
0.0600
0.0575
0.0550
0.0525
0.0500
0.0475
0.0450
0.0425
Diffuse Irradiance
2.75
2.80
2.85
2.90
2.95
3.00
3.05
3.10
3.15
3.20
Junge Parameter

(f)

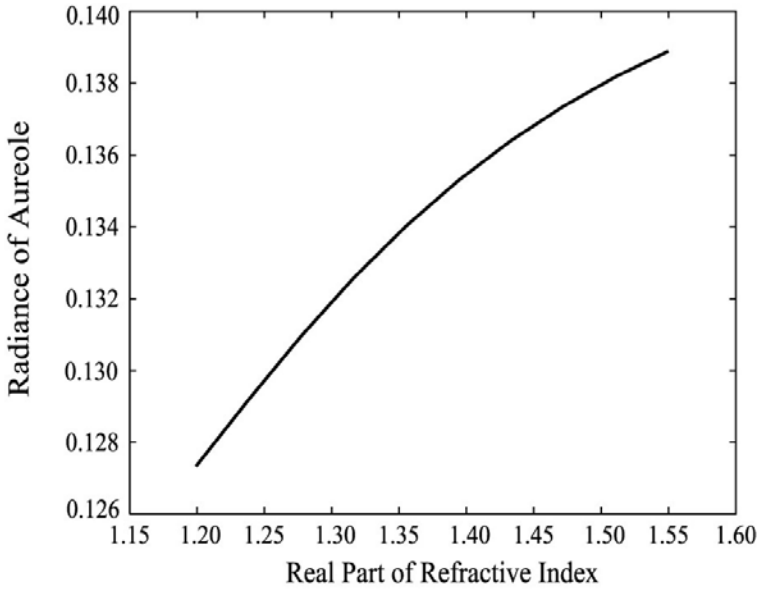
Radiance of Aureole
0.140
0.138
0.136
0.134
0.132
0.130
0.128
0.126
1.15 1.20 1.25 1.30 1.35 1.40 1.45 1.50 1.55 1.60
Real Part of Refractive Index

(g)

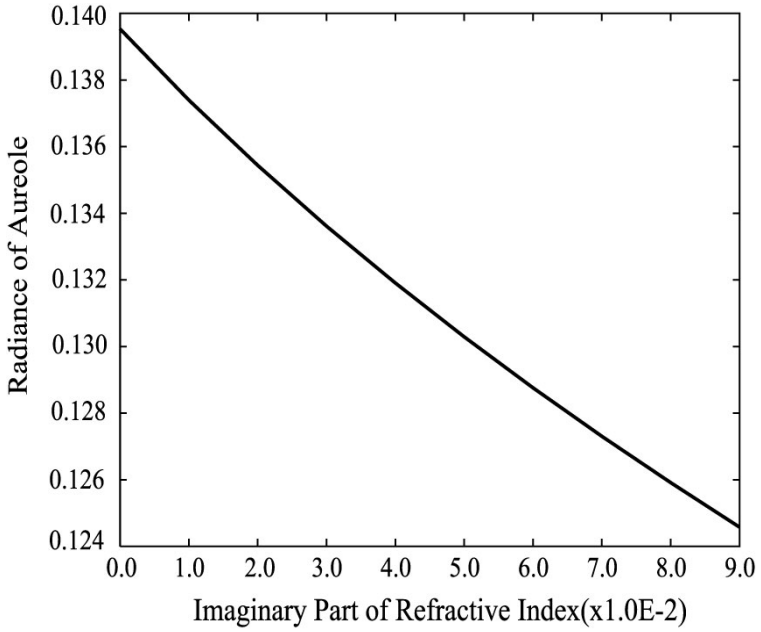
Radiance of Aureole
0.140
0.138
0.136
0.134
0.132
0.130
0.128
0.126
0.124
0.0 1.0 2.0 3.0 4.0 5.0 6.0 7.0 8.0 9.0
Imaginary Part of Refractive Index(x1.0E-2)

(h)

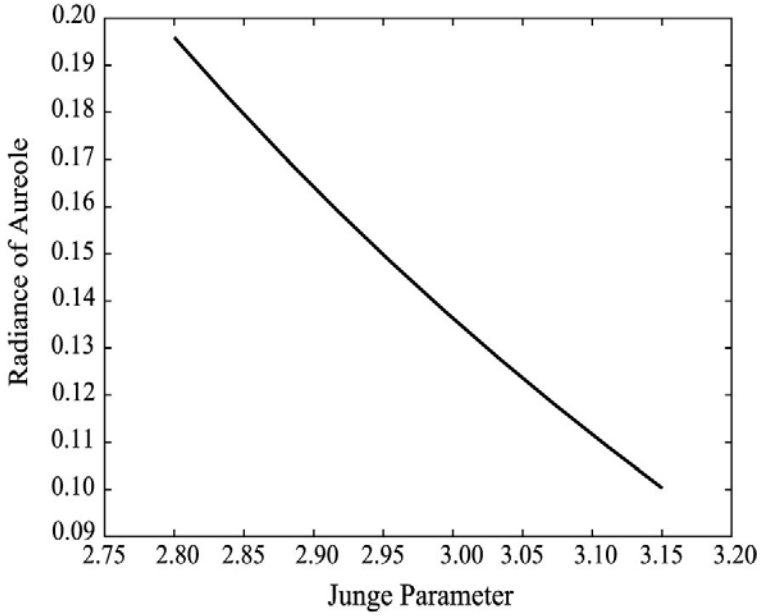

(i)

Fig.6. 2 The Dependence of the Measurement data on the parameters. (a), (b) and (c) show the dependence of the optical depth of aerosol on the real part, imaginary part and Junge parameter. (d), (e) and (f) show the dependence of the diffuse irradiance on their parameters. (g), (h) and (i) show the dependence of the aureole irradiance on their parameters.

Table 6. 2 The Sensitivities of Diffuse Irradiance, Aerosol Optical Depth and Aureole with Respect to the Real Part and the Imaginary Part of Refractive Index as well as Junge Parameter.

	Real part	Imaginary part	Junge Parameter
Diffuse solar irradiance	0.0485	0.00252	0.289
Optical depth	0.422	0.00386	0.401
Aureole	0.0676	0.00186	0.620

From Fig.6.2, we can conclude some points as follows. Firstly, the aerosol optical depth is getting larger with increasing of the real part of refractive index, but getting smaller with increasing of the imaginary part and Junge parameter. Secondly, the aureole and diffuse irradiance increase in accordance as the real part increases. On the other hand, the aureole and the diffuse irradiance decrease as the imaginary part or Junge parameter decreases. The real part corresponds to the refractive index so that the aureole and the diffuse irradiance are large if the refraction gets large because scattering increases while the imaginary part corresponds to absorption so that the aureole and diffuse irradiance are small if the absorption becomes large. Finally, the aureole and diffuse irradiance can be considered to be getting smaller if Junge parameter becomes larger because it commonly implies a case of clear atmosphere.

From table 6.2, we can find that there are great differences in the sensitivities of the measurement data on the parameters, the retrieval accuracies of the unknown parameters in which the sensitivities of the measurement data are high are excellent, but the other accuracies improvement can not be expected. The table shows that the lowest sensitivity of the measurement data to the imaginary part of refractive index results in relatively poor retrieval accuracy of the imaginary part of refractive index in Sherbrooke model.

Chapter 7

Proposed Method(Arai-Ryo Model)

Low retrieval accuracy of the imaginary part of refractive index in Sherbrooke model is due to small sensitivities of the measurement data to the imaginary part of refractive index. Meanwhile, it is also due to the linear relation between the measurement data and the unknown parameters in Sherbrooke model. To solve the problem, a multistage method (Arai-Ryo model) is proposed which is based on a combination with the nonlinear inversed method(the method of simulated annealing) and Sherbrooke model.

7.1 Introduction of the Multistage Method

Because the sensitivities of the measurement data to the imaginary part of refractive index are small so that it is difficult to obtain a high estimation accuracy for the imaginary part of refractive index while the sensitivities of the real part of refractive index and Junge parameter are good enough in Sherbrooke model. Furthermore, if the two parameters are set as constant, it could not be expected to improve the retrieval accuracy of the imaginary part of refractive index because of small freedoms. For this reason, a multistage method of which first we keep Junge parameter which is retrieved in advance by Sherbrooke model, then we estimate the real part and the imaginary part of refractive index. Here we refer to Arai-Ryo model.

That is, first, the unknown vector

$$\begin{pmatrix} \kappa \\ \eta \\ a \end{pmatrix} \tag{7.1}$$

is assumed while the measurement data with the constraint conditions are assumed as

follows,

$$\begin{aligned}
\left(\tau_{aer} - \tau^*_{aer}\right)/\tau^*_{aer} &< e_1 \\
\left(I_{dif} - I^*_{dif}\right)/I^*_{dif} &< e_2 \\
\left(I_{aue} - I^*_{aur}\right)/I^*_{aur} &< e_3
\end{aligned} \tag{7.2}$$

The estimation errors are normalized and the solution is restricted in this way so that three of measurement data can be handled on the equality of status. In these calculation, e_1, e_2, e_3 are set to be $e_1 = 10^{-5}$, $e_2 = 10^{-5}$, $e_3 = 10^{-7}$, respectively, in an empirical manner. In this iterative method, the simulated-annealing (Arai et al,1998) is used as the one of the nonlinear optimum method. We summarized this method at next section.

7.2 Method of Simulated Annealing

Simulated annealing is a global optimization method that distinguishes between different local optima. The algorithm is that an initial state is chosen at initial energy and temperature, holding temperature constant the initial state is perturbed with a perturbed function(i.e., generating function), and the change in energy is computed. The new state is accepted with a probability given by the Metropolis criteria(i.e., acceptance function). This processes is then repeated sufficient times to reach a balance expressed by a Boltzmann Distribution for the current temperature, then the temperature is decremented and the entire process repeated until the termination condition is satisfied, or a frozen state is achieved as temperature becomes 0.

7.2.1 Boltzmann Distribution and Generating function

In a certain temperature constant, the processes must be repeated sufficient times so that the energy reach a balance expressed by a Boltzmann Distribution, that is,

$$Q(x) = \exp(-F(x)/T)/Z \tag{7.3}$$

$$Z = \sum_x \exp(-F(x)/T) \tag{7.4}$$

where x represents the variable of real part, imaginary part and Junge parameter. From

the Boltzmann distribution, we can find that the probability of low energy state is rather higher when the temperature becomes low. Furthermore, only the state probability of the lowest energy is not zero as the temperature reaches a limited point($T \to 0$). Here, we introduced a generating function with a random numbers to generate next state as follows,

$$m^{l+1} = m^{l} + y_l(M_{\max} - M_{\min}) \qquad m \in [M_{\min}, M_{\max}] \tag{7.5}$$

$$y_l = sign(\mu - 1/2)T_j[(1+1/T_j)^{|2\mu-1|} - 1] \quad \mu \in [0,1]$$

where m is the vector of the real part and the imaginary part of refractive index, and $M_{\min}, M_{\max}$ are their range. l represents generated times of new state and j is the number of temperature change. μ is random from 0 to 1. The reason for introducing this generating function is that the new state is not only perturbed randomly at the previous state in their range but also affected by the cooling temperature T_j. The perturbed range of new state becomes smaller as the temperature decreases. Thus it can assure that the imaginary part with lower sensitivity reach a good precision by restricting the perturbed range of the real part with high sensitivity to nearly 0 as the temperature becomes extremely low.

In order to satisfy Boltzmann distribution or reach a balance of energy at a temperature constant, we take acceptance times large enough to make the current movement stable. The acceptance times is acceptance numbers by acceptance function which is described as following section.

7.2.2 Acceptance function

Acceptance function confirms if a new state may replace the last state at a certain temperature. It is made by the Metropolis criteria. That is,

$$A(\Delta E, T) = \begin{cases} 1 & F_{k+1} \le F_k \\ \dfrac{1}{1+\exp(\Delta E / T)} \approx \exp(-\Delta E / T) & F_{k+1} > F_k \end{cases} \tag{7.6}$$

This also satisfies inhomogeneous Markov chain, and means that next state move is only decided by the last state and temperature. From Eq.(7.6), we also can find that

every state probability are high and similar as the temperature is high, and it approximate an average value. This means that there are same chances that the current state moves to the next state event if the next state may be a high energy state. On the other hand, the probability that move to high energy state is getting lower as temperature becomes low. When the temperature approximate zero, the probability of all states become zero except for the lowest energy state. Thus we can obtain the global optima as the temperature reduces to zero.

In this thesis, the number of the measurement data is 3, this also means that three energy costs(ΔE_{τ} , ΔE_{dif} , ΔE_{aur}) exist, by using the minmax method, we can rewrite the acceptance function as follows,

$$A(\Delta E, T) = \begin{cases} 1 & F_{k+1} \le F_k \\ \dfrac{1}{1+\exp(Max(\Delta E_{\tau}, \Delta E_{dif}, \Delta E_{aur})/T)} & F_{k+1} > F_k \end{cases} \qquad (7.7)$$

7.2.3 Modified Annealing Temperature

In general, annealing temperature can be set a monotonous decreased function in learning process such as,

$$T = \frac{T_0}{\ln(t+2)} \qquad (7.8)$$

If we assume T_0 as 1.0, we can illustrate the temperature curve in Fig.7.1. We can obtain the global minima theoretically when T reduce to 0, from Fig.7.1, but, it will consume an anomalous computing resources as temperature approach to 0. It is not suitable for a practical computation.

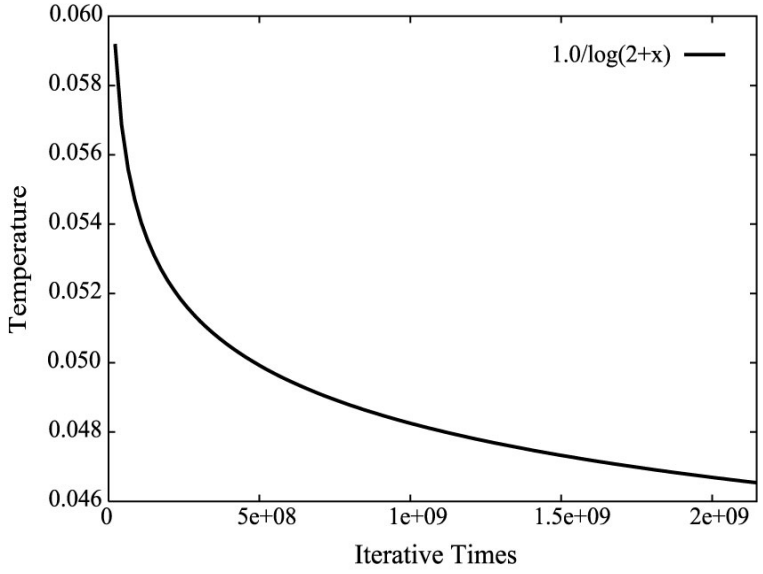

Fig.7. 1 Iterative Times Dependence on the Annealing Temperature.

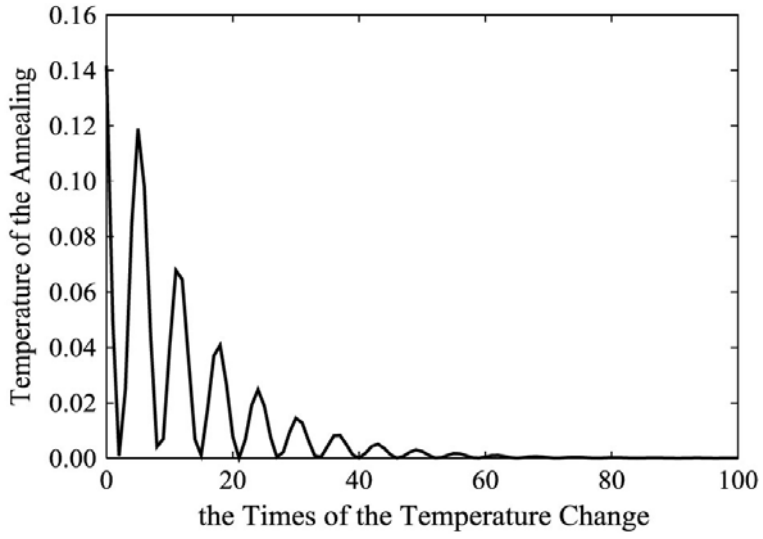

Fig.7. 2 The Annealing Temperature on Arai-Ryo Model.

In our paper, we use a decreasing oscillation function on the cooling schedule,

probability for reaching global optimum solution in an efficient way is get high enough. The proposed cooling function is as follows,

$$T_j = 0.92 * T_{j-1}(1+\cos(j+1))/2 \tag{7.9}$$

The cooling schedule is a decreasing oscilation function shown in Fig.7.2. The coefficient of 0.92 in the Eq.(7.9), is optimized in an empirical manner.

7.3 Algorithm of Arai-Ryo Model

Combining the method of simulated annealing with Sherbrooke model to our proposed method, we give an algorithm with a multistage method as follows,

1. Estimate Junge parameter using Sherbrooke model, and obtain higher accurate solution a_*
2. Set Junge parameter as a_* , set annealing temperature T, initial solution $\{\kappa_0 \quad \eta_0\}^T$,Calculate the measurement data(aerosol optical depth, diffuse irradiance and aureole) and error(e).
3. Generate new solution $\{\kappa_l \quad \eta_l\}^T$ using Eq(7.5), calculate their measurement data and error(e). According to the acceptance function Eq(7.7), confirm the state if to be accepted. This is,

   If $A(\Delta E, T)$=1 or $P(l) < \dfrac{1}{1+\exp(Max(\Delta E_\tau, \Delta E_{dif}, \Delta E_{aur})/T)}$,

   then replace $\{\kappa_{l-1} \quad \eta_{l-1}\}^T$ with $\{\kappa_l \quad \eta_l\}^T$.

   else remove $\{\kappa_l \quad \eta_l\}^T$.

4. Update T. if T=0 or $e_1 < 10^{-5}, e_2 < 10^{-5}, e_3 < 10^{-7}$, exit ,else repeat to 4.

The whole retrieval scheme based on the method of simulated annealing is simple and summarized in Fig.7.3.

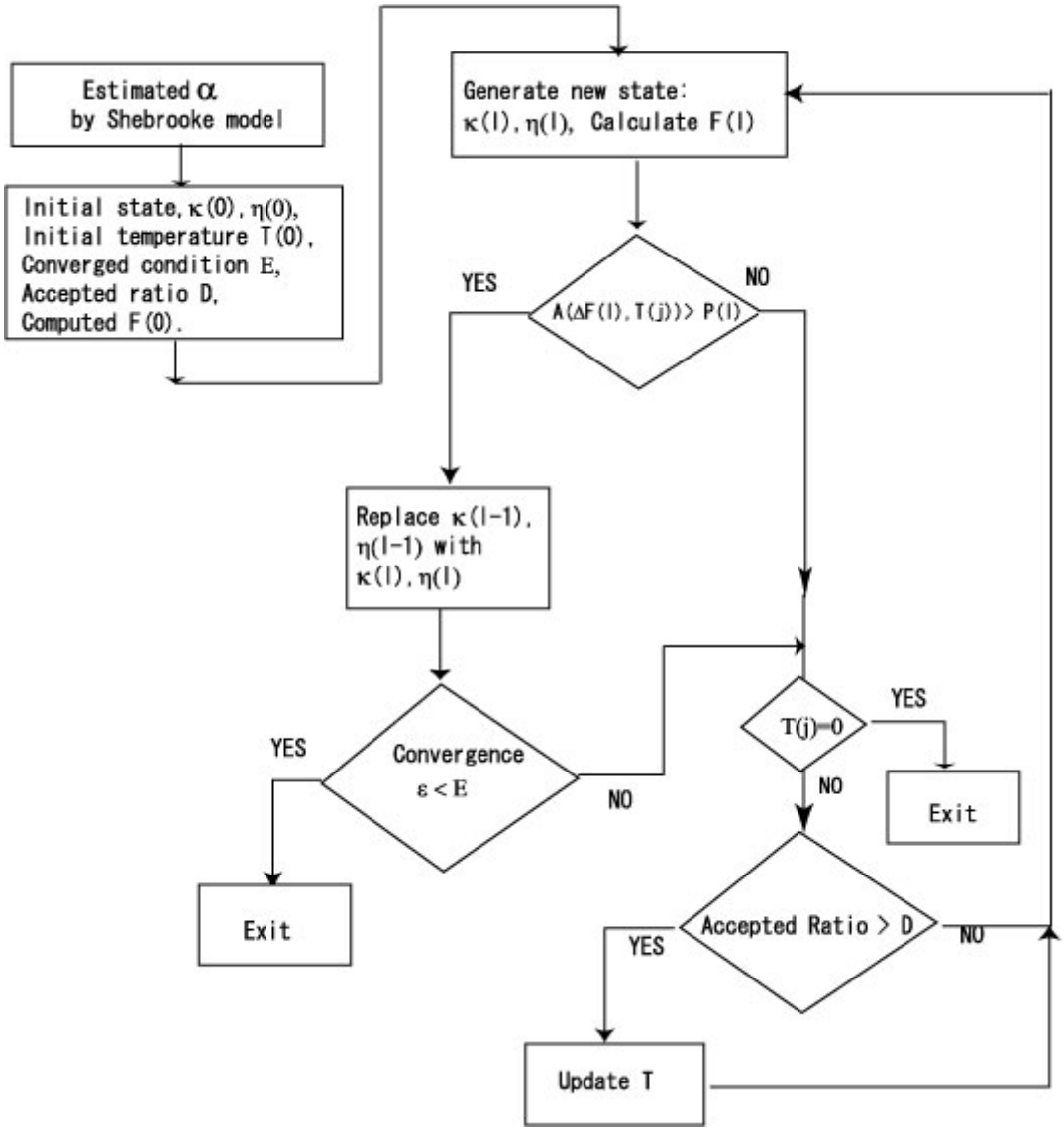

Fig.7. 3 Schematic description of Arai-Ryo model.

Chapter 8

Error Analysis

We will give an error analysis of the retrieval result in both models. In order to prove the precision of retrieval result in Arai-Ryo model, we also introduced Gauss-Seidel model which is a code to calculate the atmospheric radiative transfer developed by University of Arizona.

8.1 Comparison of Retrieval Error Between Proposed Method and Sherbrooke Model

In Fig.8.1, it shows that the real part of refractive index dependence of the diffuse solar irradiance calculated by Arai-Ryo model and by Gauss-Seidel model(Lenoble ,1985) as the imaginary part of refractive index was set 0.003 and 0.006. Junge parameter was unified on the retrieval of the diffuse solar irradiance by both models. With respect to the Gauss Seidel model, we calculate the diffuse solar irradiance using the real part and the imaginary part of refractive index as parameters by the method of successive orders of scattering. On the other hand, with respect to the retrieval of the diffuse solar irradiance by Arai-Ryo model, we gave a unified Junge parameter, a real part and an imaginary part of refractive index, and put their parameters into the constraint that the normalized retrieval accuracies of the measurement data of aureole irradiance, diffuse solar irradiance and aerosol optical depth.

In Fig.8.1, it is found that the retrieval results of both models are reasonably consistent in the range of the real part of aerosol refractive index. The error of retrieval results between the two models are not more than 2%. In this thesis, the refractive index is set as 1.53-0.007i and Junge parameter is set as 3.00, which is represented a terrestrial aerosol type. The calculated accuracies (i.e. the difference between set values from Gauss-Seidel model and retrieved values from Arai-Ryo model) of the diffuse solar irradiance and aerosol optical depth are shown in Table 8.1.

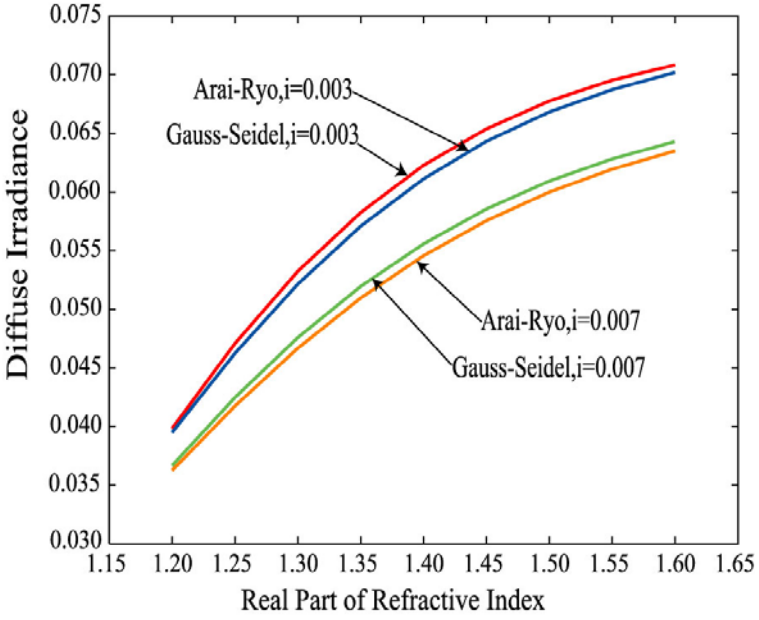

Fig.8. 1 A Comparison of Diffuse Irradiance for Arai-Ryo and Gauss-Seidel Models.

Table 8. 1 Calculated Errors on Diffuse irradiance and Optical Depth.

	Arai-Ryo	Gauss-Seidel	Estimation Error
Diffuse solar irradiance	0.05976	0.06011	0.58230%
Optical depth	0.181564	0.18157	0.00330%

Table 8.2 shows the comparison of the retrieval errors between Arai-Ryo model and Sherbrooke model. It is found that the retrieval error of the real part of

refractive index from Arai-Ryo model is lower than it from Sherbrooke model while the estimation error of the imaginary part of refractive index in Arai-Ryo model is reduced a half compared to it from Sherbrooke model.

Table 8. 2 Retieval Errors of Refractive Index and Junge Parameter.

	Designated	Sherbrooke	%	Arai-Ryo	%
Real Part	1.530	1.52964	0.023	1.52972	0.018
Imaginary Part	0.007	0.00583	16.640	0.00756	7.997
Junge parameter	3.000	2.988	0.407	2.988	0.407

* % Denotes percent difference between designated and estimated values.

The retrieval errors of the measurement data are shown in Table 8.3. The errors of the diffuse solar irradiance and the aerosol optical depth are larger much than the error of aureole irradiance in Sherbrooke model. On the other hand, it is also found that these errors decreased greatly and almost kept the same in Arai-Ryo model. It is due to the fact that the possible solutions are restricted with retrieved error norm in the Sherbrooke model while those are constricted in normalized retrieval error in Arai-Ryo model.

Table 8. 3 Retieval Errors of Diffuse irradiance, Optical Depth and Aureole.

	Sherbrooke	Arai-Ryo
Diffuse solar irradiance	2.001%	0.511%
Optical depth	1.919%	0.504%
Aureole	0.739%	0.512%

8.2 Influence Due to Surface Reflectance and Convergence Process

Until now the surface reflectance is assumed as 0, naturally, the retrieval accuracies are influenced since the multiple-scattering in the atmosphere and multiple-reflection from the surface become large if the surface reflectance increases. Assuming Junge parameter to be 3.0, the aerosol refractive index to be 1.53-0.007i, influence of the surface reflectance is evaluated at Table 8.4. It is found that the retrieval accuracies are almost similar as the surface reflectance increases in Arai-Ryo model.

Table 8. 4 Influence Due to Surface Reflectance on Retieval Errors of Diffuse Irradiance, Optical Depth and Aureole

Surface reflectance	0.0	0.1	0.2
Diffuse solar irradiance	0.530%	0.511%	0.511%
Optical depth	0.528%	0.504%	0.509%
Aureole	0.530%	0.512%	0.511%

Naturally, the time required for the convergence in the Arai-Ryo model is far more than that of Sherbrooke model. A comparison is shown in Table 8.5.

Table 8. 5 A Comparison of Elapsed Time

	Sherbrooke	Arai-Ryo
Elapsed time(hour)	0.03	55.30

*CPU=1GHz, Memory=128M

Fig.8.2 shows the convergence process for Arai-Ryo model, we can find that the real part becomes stable, but the imaginary part perturbs a quite large range as the temperature becomes extremely low. This is because the sensitivities of the measurement data to the imaginary part are lower much than that to the real part. Thus it can assure that the imaginary part with lower sensitivity reach a good precision by restricting the perturbed range of the real part with high sensitivity to nearly 0 as the temperature becomes extremely low. The solutions tend to local optima as the temperature reaches a lowest value. In addition, the direct irradiance perturbs larger than the aureole and diffuse irradiance during the learning process since the sensitivity of the direct irradiance to the real part is larger than that of the other two data. We obtain the best solutions as acceptence times is 1592.

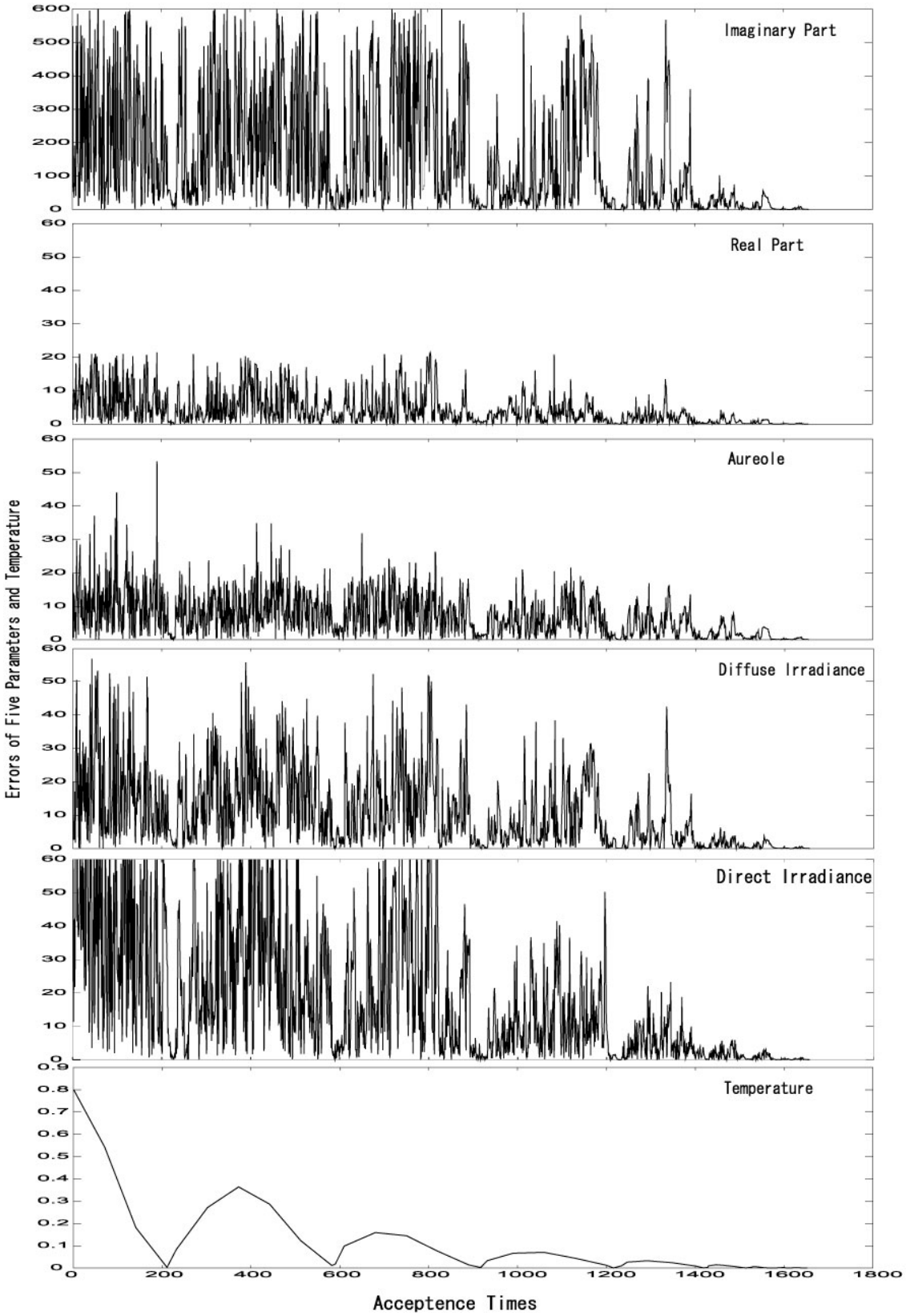

Fig.8. 2　A Example of Convergence Process for Arai-Ryo Model.

Chapter 9

Conclusion

It is found that the retrieval errors of the real part and the imaginary part of refractive index and Junge parameter are 0.0299%, 16.64%, 0.0406%, respectively, for the Sherbrooke model. The retrieval precision of the imaginary part of the refractive index is extremely low than that of the real part and the Junge parameter. Through a sensitivity analysis we find that it is caused by the fact that the sensitivities of the measurement data are greatly lower to the imaginary part of refractive index than the other two parameters. On the other hand, comparison to the retrieval errors from Sherbrooke model, it is found that the error of the real part of refractive index becomes small while the error of the imaginary part is reduced more than a half in the Arai-Ryo model. It is due to the fact that the relation between the unknown parameters (the refractive index and the size distribution) and the measurement data (the diffuse solar irradiance, aerosol optical depth and aureole) is not linear.

Additionally, the three measurement data can be handled on equality status because the solution lei on constraints with the normalized retrieval errors of the measurement data in Arai-Ryo model. Meanwhile, because these errors are not normalized in Sherbrooke model so that it is found that the retrieval error of the diffuse solar irradiance is relatively large while those errors of the aerosol optical depth and the aureole are smaller. Furthermore, it is also found that the influence due to the surface reflectance on the retrieval accuracies for Arai-Ryo model is almost the same. Even if the surface reflectance is 0.2, the retrieval accuracies of diffuse solar irradiance, aerosol optical depth and aureole for the Arai-Ryo model are around 0.5% and are still superior to that for the Sherbrooke model which is about 2.0%.

Reference

[1] 新井康平、梁興明、シミュレーテッドアニーリングによる太陽直達，散乱および周縁光を用いたエアロゾルの複素屈折率および粒径分布の同時推定, 日本リモートセンシング学会誌、Vol.23, No.1, pp.11-20，2003.

[2] K.Arai and Xing Ming Liang, Method for estimation of refractive index and size distribution of aerosol using direct and diffuse solar irradiance and aureole by means of simulated annealing, Advances in Space Research, Vol.32, No.11, pp.2165-2174, 2003.

[3] K.Arai and Xing Ming Liang, Method for estimation of refractive index and size distribution of aerosol using direct, diffuse and aureole by means of simulated annealing. Proceddings of the COSPAR (Committee on Space Research) Congress, p.10 (Solicited Paper), Texas, USA, Oct., 2002.

[4] K.Arai, Y.Iisasa and Xing Ming Liang, Aerosol parameter estimation with changing observation angle of ground based polarization radiometer, Proc.of the COSPAR Congress(Paris), A-00579,A3.1-0037-04, July 2004.

[5] K.Arai and Xing Ming Liang, Characterization of aerosols in Saga city areas in Japan with direct and diffuse solar irradiance and aureole observations, Proc.of the COSPAR Congress(Paris), A-00582, A1.1-0130-04, July 2004.

[6] 新井康平、梁　興明、非線形逆問題解法に基づく太陽直達、散乱および周縁光によるエアロゾル粒径分布および複素屈折率推定、日本リモートセンシング学会第 33 回学術講演会、佐賀大学、pp. 145-146、2002 年 11 月 28, 29 日

[7] 新井康平，梁興明、非線型逆問題解法に基づく太陽直達，散乱および周縁光によるエアロゾル粒径分布，複素屈折率推定、日本リモートセンシング学会第 34 回学術講演会，pp. 209-210、2003 年 5 月 16 日

[8] Romanov, P., Norman T.O'Neill and A.Royer, Simultaneous retrival of aerosol refactive index and particle size distribution from ground-based measurements of direct and scattered solar radiation, Applied Optics, Vol. 38, No. 36, pp.7305-7320,1999.

[9] 新井康平、リモートセンシングの基礎理論、学術図書出版社、2001.

[10] 竹内延夫、地球大気の分光リモートセンシング、学会出版センター、2001.

[11] Guang-Yu Shi, Ground-based measurements of aerosol parameters, Institute of atmospheric Physics, Chinese Academy of Science, G-0063 second progress report,1998

[12] I.Lenoble, Radiative transfer in scattering and absorption atmospheres, A. DEEPAK Publishing, 1985.

[13] Shunlin liang, Quantitative remote sensing of land surface, John Wiley & Sons, Inc, 2004.

[14] Box,M.A. and A.DEEPAk, An approximation to multiple scattering in earth's atmosphere: Almucantar irradiance formulation, Journal of atmospheric science,Vol.38, pp.1037-1048,1981.

[15] Deirmendjian,D.,Theory of solar aureole,Part Ⅱ,application to atmospheric models, ann.Geophys., vol.15, pp.218-249,1959.

[16] McClatchey,R.A.,R.W.Fenn,J.E.A.Selby,F.E.Volz and J.S.Garing, Optical properties of the atmosphere(3rd ed.). AFCRL Envirn.Res.Papers No.411, pp108.,1972.

[17] Arai,K and Y.Minematsu, Image restoration based on maximum entropy method with parameter estimation by annealing, Journal of the Japanese photogrametry and remote sensing society, Vol. 37, No. 2, pp.15-22,1998.

Acknowledgement

Author wishes to express deep gratitude to the lead teacher, Professor K. Arai, for his valuable guidance and teaching.

Author wishs to thank Professor Yamasita, Associate Professor Okumura, Teaching Assistant Terayama, Teaching Assistant Eto and Technology Stuff Koujima, for their valuable guidance and support.

Author also thanks all of the members of the department of information science, Saga University, for their support.